PARIS 2017

Tu B1 02

Diffraction Modelling and Imaging of Fluid Escape Features, South China Sea

T.J. Moser* (Moser Geophysical Services), M.A. Pelissier (Integrated Geoscience Solutions), A. Ball (Roc Oil (China)), I. Sturzu (Z-Terra Inc.), A.M. Popovici (Z-Terra Inc.)

Summary

This paper investigates the seismic diffraction response of fluid escape features and their impact in diffraction imaging. Since fluid escape features are generally vertically aligned scattering objects, diffraction imaging has an illumination uplift compared to regular reflection depth migration. We compare diffraction modeling and imaging on concept models of fluid escape pipes with results to those of a South China Sea data set. The polarity reversal and tuning properties of diffraction imaging turn out to have important implications for detectability and resolution of fluid escape pipes and the interpretation of fluid migration and trap charging.

Introduction

Fluid escape pipes on 3D seismic data have been studied extensively in recent years, beginning with a paper by Løseth et al. (2001) on gas blow-out pipes in Nigeria. These features are typically interpreted on conventional reflection seismic images. In this paper we investigate the application of diffraction imaging for the detection and resolution of fluid escape pipes. We first use synthetic data to model the diffraction imaging response and then compare the results to those of a South China Sea data set.

Diffractions are the seismic response from subsurface discontinuities. Unlike reflections, diffractions do not satisfy Snell's specular reflection law. As such, diffractions can be regarded as the carrier of information from non-reflecting small-scale features, such as small faults, fractures, pinch-outs, salt-flanks, karst features and injectites. As noted by Løseth et al. (2011), the reflector terminations against the edges of a pipe produces diffractions. Moser et al. (2016) study the diffraction response of vertically aligned objects such as natural pipes and man-made boreholes.

The Diffraction Imaging Method

The objective of diffraction imaging is to isolate subsurface discontinuities and image these separately from standard migration. Typically this is done in a pre-stack migration framework, where a migration weight is applied inside the migration loops, suppressing reflection energy that satisfies Snell's law and enhancing diffraction energy that does not. Diffraction images are used as a complement to the structural images produced by conventional reflection imaging techniques, by emphasizing small-scale structural elements that are difficult to interpret on a conventional depth image. A key component in the diffraction imaging workflow is the specularity gather analysis which allows to generate diffraction images with various degrees of reflectivity suppression (Sturzu et al. 2013).

Two main benefits of diffraction imaging are high resolution imaging and superior illumination (Khaidukov, Landa and Moser, 2004; Sturzu et al. 2013). The high-resolution potential of diffraction imaging is demonstrated by numerous case histories in carbonate reservoirs and unconventional shales, where the diffraction images show much more structural detail than conventional depth migration or coherence (Sturzu et al. 2014). Pelissier et al. (2015) use diffraction imaging to obtain a better fault definition in a field which is highly compartmentalized by complex faulting. The illumination potential is demonstrated by the imaging of vertically aligned objects such as fluid escape features, which are unfavourable to normal reflection processing.

Modelling of the seismic diffraction response of fluid escape pipes

A 2D sketch for a fixed diameter fluid escape pipe is given in Figure 1a. Each reflector termination on the pipe gives rise to an edge diffraction. A ray path diagram for the reflection and diffracted rays for a single reflector segment is shown in Figure 1b. The diffraction imaging process attenuates the specular reflection. A mild specularity taper leaves a remnant sub-specular reflection and the edge diffraction. An increasing specularity taper progressively attenuates the remnant reflection and isolates the edge diffraction.

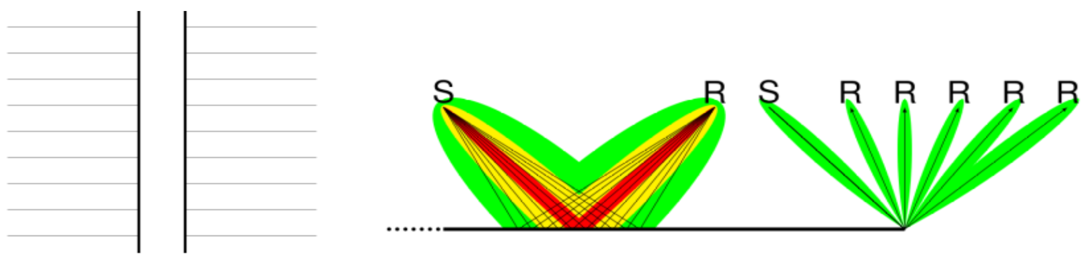

Figure 1 *a) Schematic model of fluid escape pipe b) Reflected and edge diffracted rays with Fresnel zones for specular (red), sub-specular (yellow) and non-specular (green) rays.*

The basic building block for the seismic diffraction problem is the pair of edge diffractions from opposite sides of the pipe associated with a reflector. An example of the PSDM and diffraction image is given in Figure 2a. In our model, the opposite edge diffractors have the same amplitude; this is based on the assumption that the refection amplitudes are effectively identical in the real data. A fundamental property of edge diffractions is the polarity reversal. This applies to both the forward and inverse problems. The imaged diffraction before the end of the reflector has the same polarity as that of the reflector. Beyond the edge, the polarity is opposite. These two parts have the same amplitude. For a pipe with a sufficiently large diameter there is no interference of the edge diffractors. As the diameter decreases, the interior diffractors produce an interference effect, reminiscent of the classical reflection tuning problem for a wedge model described by Widess (1973) and Kallweit and Wood (1982).

A very important characteristic of the diffraction tuning problem for the fluid escape pipes is that the interior diffractions are of the same polarity. Because of this, as the pipe diameter decreases, the diffractors first interfere constructively. This is illustrated in Figure 2b. Here the diffraction response is plotted laterally at the same depth as that of the reflector in Figure 2a. We can also see that when the diameter is such that the maximum amplitudes of the interior diffractors coincide, the resulting amplitude doubles. As the diameter decreases further, the edge diffraction pair begins to interfere destructively. If we rotate the wavelet shown in Figure 2b and 2c by 90 degrees, we have precisely the geometry of the classical thin bed problem described by Widess (1973), with a zero phase wavelet and two reflection coefficients of opposite polarity. Now consider the sum of the two wavelets shown in Figure 2b or 2c for a range of pipe diameters. Taking the maximum positive amplitude, we obtain the *amplitude tuning curve* shown in blue in Figure 2d. If we instead rotate the wavelet by 90 degrees, we obtain another amplitude tuning curve shown in black. Using the instantaneous amplitude defined by Taner, Koehler and Sheriff (1979), we obtain an *envelope tuning curve* shown in red. Since the envelope is invariant to phase, the envelope tuning curve represents the maximum possible amplitude for the family of amplitude tuning curves associated with various phase rotations. From this, we observe that the amplitude tuning curve for the pipe diffraction provides the highest possible constructive interference, and this is relatively higher than the level of tuning in the Widess model for reflection. Therefore the pipe diffraction model provides the highest possible level of constructive interference. For the thin bed reflection problem, a doubling in amplitude can only be achieved if the top and base reflectors have the sample magnitude and polarity, as shown by Kallweit and Wood (1982).

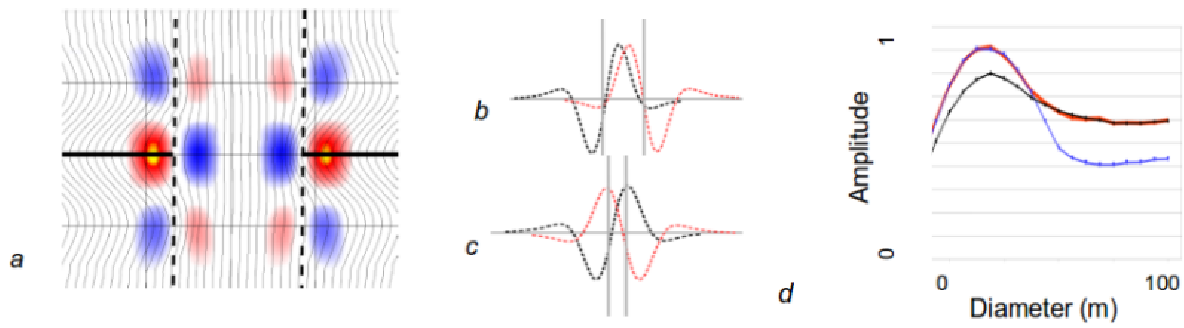

***Figure 2** a). PSDM (wiggle) and diffraction image (colour) for an 80m diameter pipe b) diffraction response at the reflector depth, plotted laterally, for a diameter which results in constructive interference c) smaller diameter associated with destructive interference d) tuning curves .*

The imaged response for a range of pipe diameters is shown in Figure 3. The diffraction energy present on the PSDM is noticeably weaker than the reflection energy; as the diameter decreases, the diffraction response could readily be obscured by noise in the real data. On the diffraction image, we observe amplitude variations due to tuning. The application of the specularity taper shown in Figure 3c allows for the interpretation of both non-specular reflections and diffractions. The attenuation of the specular reflection increases the relative strength of the diffractions. The diffraction strength is further enhanced for some diameters by constructive interference. For all diameters, the polarity reversal provides a strong contrast with the phase of the remnant reflectors. Note that although the trace spacing is 25 m, a 5 m pipe is clearly resolved by the diffraction imaging, since the edge diffractors are less subject to the illumination restrictions of Snell's law. Furthermore, below tuning, the diffraction interference exaggerates the pipe diameter; this is similar to the known observation that reflection interference exaggerates a thin bed's thickness below tuning.

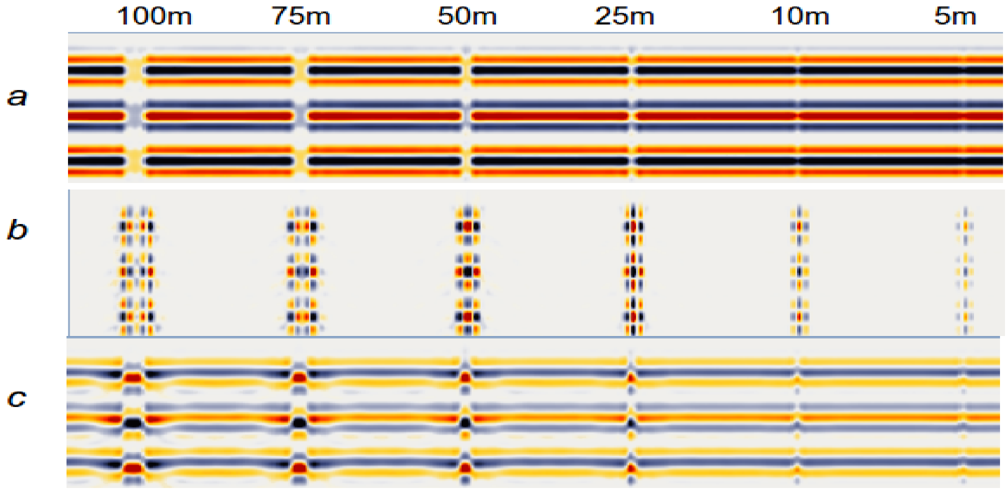

Figure 3 *a) PSDM b) diffraction images c) Specularity taper of 99.5 %. Trace spacing 25 m. Peak frequency 20 Hz.*

South China Sea Example

An example from the South China Sea is shown in Figure 4. Here we can clearly observe the increased amplitude as well as the polarity reversal on the seismic section and depth slice.

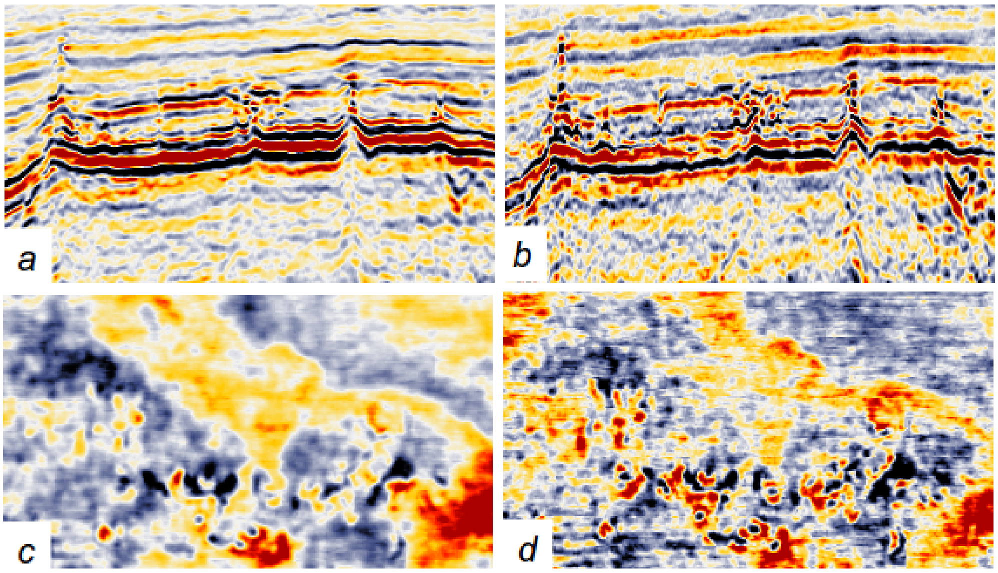

Figure 4 *a) PSDM inline , b) DI taper 99.5%. c) PSDM depth slice, d) DI depth slice taper 98%.*

The instantaneous amplitude envelope of the diffraction image is also a useful attribute for the characterization of fluid escape pipes. The amplitude envelope is invariant to the polarity of the imaged diffractors and at the same time is sensitive to the vertical their vertical stacking pattern. The amplitude envelope can help in the detection of closely spaced pipes.

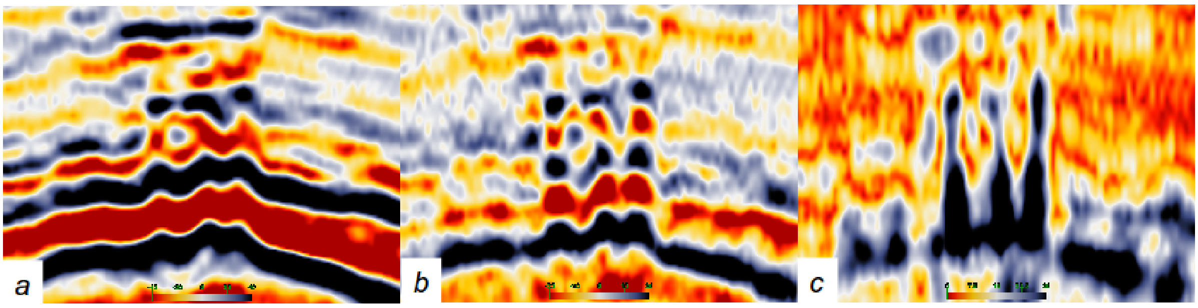

Figure 5 *a) PSDM b) DI tapered at 98% c) Envelope of diffraction image.*

Conclusions

The polarity reversal and tuning are key elements of the seismic diffraction response of fluid escape pipes. At the pipe diameter corresponding to maximum constructive interference, the diffraction amplitude doubles. These two effects combine to provide a distinctive signature on the diffraction image which significantly improved detectability and resolution over the conventional reflection seismic image.

The diffraction imaging of South China Sea dataset confirms the modelling results. This has important implications for the detectability and resolution of fluid escape pipes and the interpretation of fluid migration and trap charging.

Acknowledgements

The authors would like to thank the data owners for permission to show the South China Sea example.

References

Kallweit, R.S and L.C. Wood, 1982, The limits of resolution of zero-phase wavelets., *Geophysics* **47**, 1035-1046.

Khaidukov V., Landa E. and Moser T.J. 2004. Diffraction imaging by focusing-defocusing: An outlook on seismic superresolution, *Geophysics*, **69**, 1478-1490.

Løseth H., Wensaas L., Arntsen B., Hanken N., Basire C. and Graue K. 2001. 1000m long gas blow-out pipes, *63rd EAGE Conference and Exhibition, Amsterdam*.

Løseth H., Wensaas L.,Arntsen B., Hanken N., Basire C. and Graue K. 2011. 1000m long gas blow-out pipes, *Marine and Petroleum Geology*, **28**, 1047-1060.

Moser T.J., Arntsen B., Johansen S., Raknes E.B. and Sangesland S. 2016. Seismic Diffraction Response from Boreholes, *78th EAGE Conference, Vienna.*

Pelissier M.A., Moser T.J., Jing L., de Groot P., Sirazhiev A., Sturzu I. and Popovici A.M. 2015. Diffraction Imaging of the Zhao Dong Field, Bohai Bay, China, *77th EAGE Conference, Madrid*.

Sturzu I., Popovici A.M., Tanushev N., Musat I., Pelissier M.A. and Moser T.J. 2013. Specularity Gathers for Diffraction Imaging, *75th EAGE Conference, London*.

Sturzu I., Popovici A.M., Pelissier M.A., Wolak J.M. and Moser T.J. 2014. Diffraction imaging of the Eagle Ford shale, *First Break*, **32**, 49-59.

Taner M. T., Koehler F. and Sheriff R. E., 1979. Complex seismic trace analysis, *Geophysics*, **44**, 1041-1063.

Widess, M. B., 1973. How thin is a thin bed?, *Geophysics*, **38**, 1176-1180.